Biosensors and Bioelectronics 126 (2019) 151–159

Contents lists available at ScienceDirect

Biosensors and Bioelectronics

journal homepage: www.elsevier.com/locate/bios

A dual-signal readout enzyme-free immunosensor based on hybridization chain reaction-assisted formation of copper nanoparticles for the detection of microcystin-LR

Zuyu He[a,b], Yue Cai[a], Ziming Yang[b], Puwang Li[b], Hongtao Lei[c], Weipeng Liu[a,*], Yingju Liu[a,*]

[a] College of Materials & Energy, South China Agricultural University, Guangzhou 510642, China
[b] Agriculture Products Processing Research Institute, Chinese Academy of Tropical Agricultural Sciences, Zhanjiang 524001, China
[c] The Guangdong Provincial Key Laboratory of Food Quality and Safety, College of Food Science, South China Agricultural University, Guangzhou 510642, China

ARTICLE INFO

Keywords:
Immunoassay
Dual-signal readout
Hybridization chain reaction
Microcystin-LR

ABSTRACT

Enzyme-based electrochemical biosensors are widely used in immunoassays, but the intrinsic disadvantages of enzymes including instability or sensitivity to temperature and pH should be considered. Herein, an enzyme-free and dual-signal readout immunoassay was established to detect microcystin-LR (MC-LR) sensitively and selectively. Firstly, the microplate was modified with gold nanoparticles-decorated-carbon nanotubes (AuNP-CNT) to immobilize sufficient antigens by the high surface area of CNT and high affinity of AuNP. Then, silver nanoparticles were decorated on gold nanorods to form corn-like AgNP/AuNR composite and then capture secondary antibody and initiator DNA strand. After hybridization chain reaction, long double helix DNA strands can be formed on AgNP/AuNR to germinate copper nanoparticles. A dual-signal readout from the current responses of both silver and copper ions was obtained by using differential pulse stripping voltammetry with the aid of acid-treatment. By using a competitive immunoreaction, MC-LR can be detected in a linear range from 0.005 μg/L to 20 μg/L with a lower detection limit of 2.8 ng/L. The reproducibility, stability and specificity were all acceptable, indicating its promising application in environment monitoring and sensitive electrochemical detection for other analytes.

1. Introduction

Microcystins (MCs), a family of cyclic heptapeptide toxins produced by several genera of cyanobacteria in water environment, can cause severe human health problems due to their hepatotoxic and tumor-promoting activities (Pham and Utsumi, 2018). Microcystin-LR (MC-LR), as one of the most toxic byproducts of cyanobacteria among MCs (Karci et al., 2018), has been recommended no more than 1 μg/L in drinking water by World Health Organization. Up to now, many methods have been developed to detect MC-LR, including high-performance liquid chromatography (Zhang et al., 2004a), liquid chromatography-mass spectrometry (Ríos et al., 2013), protein phosphatase inhibition assays (Noble et al., 2003) and Raman spectroscopy (Halvorson and Vikesland, 2011). However, expensive instruments, skilled technicians and complicated pretreatment restrict their popularization. Therefore, it is still worthwhile to explore a quick, precise and sensitive detection method for MC-LR. Recently, electrochemical immunosensors, with the advantages of high sensitivity, cost-efficiency, easy manipulation and good portability, have been used to analyze targets including biomarker (Chikkaveeraiah et al., 2012), protein (Jeong et al., 2013), pathogen (Jung et al., 2010), microorganism (Wan et al., 2011) and organic molecules (Sun et al., 2014; Qileng et al., 2018a). Thus, electrochemical immunosensors play an important role in clinic diagnosis and environment monitoring (Qileng et al., 2018b; Felix and Angnes, 2018).

Usually, electrochemical immunoassays used enzymes such as horseradish peroxidase (HRP) (Zhao et al., 2016) or alkaline phosphatase (ALP) (Yang et al., 2015) to produce the detection signal. But enzymes have intrinsic disadvantages such as high cost, instability and high sensitivity to temperature and pH (Lin et al., 2015). Recently, sensitive enzyme-free electrochemical sensors based on nanomaterials have been developed. For example, Yuan's group developed an enzyme-free electrochemical immunosensor by using poly(amidoamine) dendrimer-encapsulated gold nanoparticles as both nanocarriers and nanocatalysts, while the detection limit of procalcitonin can reach 0.36 pg/mL (Shen et al., 2015). However, many enzyme-free

* Corresponding authors.
E-mail addresses: weipeng_liu@scau.edu.cn (W. Liu), liuyingju@hotmail.com (Y. Liu).

https://doi.org/10.1016/j.bios.2018.10.033
Received 9 September 2018; Accepted 16 October 2018
Available online 19 October 2018
0956-5663/

immunoassays just replace bioenzymes by mimic enzymes that the detection condition is still rigorous and easily disturbed. Consequently, metal nanoparticles, such as silver nanoparticles (AgNPs), are used as the labels because of their sensitive response from voltammetric or stripping analysis (Lai et al., 2011). But AgNPs with small size are easily suffered from aggregation, so it is not perfect to use AgNPs as nanocarriers directly (Peng et al., 2011). Hence, it is necessary to explore materials to stabilize AgNPs or load AgNPs (Lai et al., 2012; Lin et al., 2012). Recently, gold nanorods (AuNRs), with the merits of large-scale synthesis, high surface area, long-term stability and monodispersibility, have been widely used as labeled-materials (Alagiri et al., 2017). Especially, gold nanomaterials can be conveniently functionalized with sulfydryl-modified materials by means of gold-thiolate bonds (Häkkinen, 2012). Dopamine dithiocarbamate (DDTC), synthesized from carbon disulfide and dopamine, can be absorbed onto the surface of AuNRs, while hydroxyl groups of DDTC can be served as reducing groups and growth-sites to form silver nanoparticles (Dai et al., 2017), but also as the derivate sites to combine with APTES and thus provide amino groups for biomolecule immobilization (Pivetal et al., 2017). Interestingly, not only can the thickness of silver shell be tunable by changing the amount of silver ions, but also the concentration of analytes can be quantified through stripping voltammetry after dissolving silver from AgNP/AuNR (Yin et al., 2017), which can circumvent the enzyme catalysis reaction and simplify the detection procedure.

Typically, immunosensors are established based on two components: a recognition unit to provide selective/specific binding sites for the target analytes and a transducer component for signaling the binding event to give out quantifiable signals (Kokkinos et al., 2016). It is conducive to improve the sensitivity of an immunoassay by increasing the amount of signal tags. Thus researchers have developed multifarious nanomaterials to capture as more as signal tags to amplify signal responses (Du et al., 2010; Gan et al., 2016). But the loading capacity of signal tags was restricted by the limited surface area and steric hindrance of nanocarriers (Ge et al., 2014a). Hybridization chain reaction (HCR) is an enzyme-free process that an initiator DNA strand can trigger a cascade of hybridization process when two stable species of DNA hairpins coexist in solution (Dirks and Pierce, 2004), thus a long double strand DNA (dsDNA) can be formed to amplify detection signal (Ge et al., 2014b). Especially, such DNA double strand could serve as an efficient template for the formation of copper nanoparticles (Cu NPs) (Rotaru et al., 2010). Due to the florescence of Cu NPs, Wang's group developed a label-free and non-enzymatic amplification fluorescent method to detect DNA as low as 0.4 nM (Song et al., 2014). However, it should be noted that the fluorescence emission of monomeric Cu NPs continues for only 20 min that it is not suitable for long-time monitoring application (Xu et al., 2014). Electrochemical testing is an alternative to conquer this defect by detecting cupric ion under differential pulse stripping voltammetry (DPSV) (Zhu et al., 2016).

In this work, gold nanoparticle (AuNP) modified carbon nanotube (CNT) composite (AuNP-CNT) was synthesized via one-step mild process and used as the substrate to immobilize antigens. Furthermore, AgNP/AuNR was served as the nanocarrier to conjugate with secondary antibody (Ab_2) and the initiator DNA strand. After HCR, long dsDNA was formed to provide the template for Cu NPs loading. By acid-treatment, dual-signal readout from the silver on AgNP/AuNR and the copper on dsDNA can be produced under DPSV. Thus, the competitive method was used to detect MC-LR sensitively.

2. Experimental

2.1. Materials and apparatus

CNTs were purchased from Cnano Technology Ltd. Gold (III) chloride tetrahydrate ($AuCl_3{\cdot}HCl{\cdot}4H_2O$) was bought from Shanghai Chemical Reagent Co. Ltd. Dopamine, CS_2), $NaBH_4$, $AgNO_3$ and $CuSO_4$ were from Aladdin Chemistry Co. Ltd. N-(3-dimethylaminopropyl)-N-ethylcarbodiimide hydrochloride (EDC), N-hydroxysuccinimide (NHS) and (3-aminopropyl) triethoxysilane (APTES) were bought from J&K Chemical Company. Hexadecyl trimethyl ammonium bromide (CTAB) and hexadecyl trimethyl ammonium Chloride (CTAC) were from Sigma-Aldrich Co. Ltd. The antigen and the antibody (Ab_1) of MC-LR were received from College of Food Science, South China Agricultural University. The secondary goat anti-rabbit antibody (Ab_2, 0.5 mg/mL) was bought from Abcam. MC-LR, MC-RR, MC-YR and nodularin were bought from Enzo Life Sciences Company. All biological reagents including agarose, 2-morpholinoethanesulfonic acid (MES), 3-morpholinopropanesulfonic acid (MOPS) and DNA oligonucleotides were from Shanghai Sangon Biological Engineering Technology & Services Co. Ltd. The DNA sequences of initiator DNA strand (S_0) and hairpin oligonucleotides hybridization strand (H_1 and H_2) are as follows:

S_0: 5′-CHO-$(CH_2)_6$-CCC CCC AGT TGT AGT CAG ACT ATT CGA T-3′
H_1: 5′-AGT CAG ACT ATT CGA TGC AAG TAT CGA ATA GTC TGA CTA CAA CT-3′
H_2: 5′-ACT TGC ATC GAA TAG TCT GAC TAG TTG TAG TCA GAC TAT TCG AT-3′

All electrochemical measurements were performed on CHI660E electrochemical workstation (Chenhua Instruments Co. Ltd., Shanghai, China) with glass carbon electrode (diameter of 2 mm) as working electrode, Ag/AgCl electrode as reference electrode and the platinum wire as auxiliary electrode, respectively. The UV–vis 2550 (Shimadzu, Japan) and Nicolet iS10 (Thermo Scientific, America) were employed to obtain UV–vis and FT-IR spectra, respectively. The morphologies of the materials were observed on transmission electron microscopy (JEOL, JEM-2100F) and scanning electron microscopy (SEM, QUANTA 3D FEG), and chemical status was analyzed with X-ray photoelectron spectroscopy (XPS, Thermo-VG Scientific, ESCALAB 250). Gel electrophoresis was run on DYY-6D electrophoresis apparatus (Beijing LiuYi Instrument Company, China). Zeta potential was performed on Malvern Zetasizer Nano ZSE (England).

2.2. Preparation of AuNP-CNT composite

The AuNP-CNT composite was prepared as Scheme 1B. CNT (0.2 g) was mixed with 60 mL sulfuric acid and nitric acid (3:1, v/v) under stirring at 80 °C for 5 h. In 2 mL of 1 mg/mL ox-CNT solution, 0.1 mL of 100 mM $HAuCl_4$ was added, followed by adding 0.3 mL of 50 mM ascorbic acid. After centrifugation and washing, the AuNP-CNT composite was redispered in 2 mL water for further use.

2.3. Preparation of S_0-AgNP/AuNR-Ab_2 composite

The S_0-AgNP/AuNR-Ab_2 composite was prepared as Scheme 1C. Firstly, AuNRs were synthesized (See Supporting Information). Then, DDTC was prepared by mixing 80 μL of CS_2 and 10 μL of triethylamine into 1 mL dopamine solution (0.1896 g) and then sonicating for 5 min (Mehta et al., 2013). After that, 0.8 mL of DDTC was added into 1 mL AuNR solution and stirred for 12 h, thus DDTC-modified AuNR was synthesized. Subsequently, 80 μL of 10 mM $AgNO_3$ was added and reacted at 65 °C for 4 h to form AgNP/AuNR. Finally, it was aminated by adding 20 μL of APTES into 2 mL AgNP/AuNR, stirring for 12 h, centrifugation and dispersing in 1 mL MES solution (50 mM, pH = 6.5). After the amino-modified AgNP/AuNR was sonicated for 30 min, 10 μL of Ab_2, 1 mM EDC and 2 mM NHS were added and magnetically stirred for 20 min, followed by the addition of 20 μL of 100 μM initiator DNA strand solution (S_0), and the mixture was continually stirred at 4 °C for 12 h. Thus, Ab_2 and S_0 can be covalently linked with amino-modified AgNP/AuNR through carboxyl and aldehyde group based on Schiff base reaction. The resulting S_0-AgNP/AuNR-Ab_2 composite was suspended in PBST 7.4 (10 mM PBS, pH = 7.4, containing 0.5% tween-20) after centrifugation and washing.

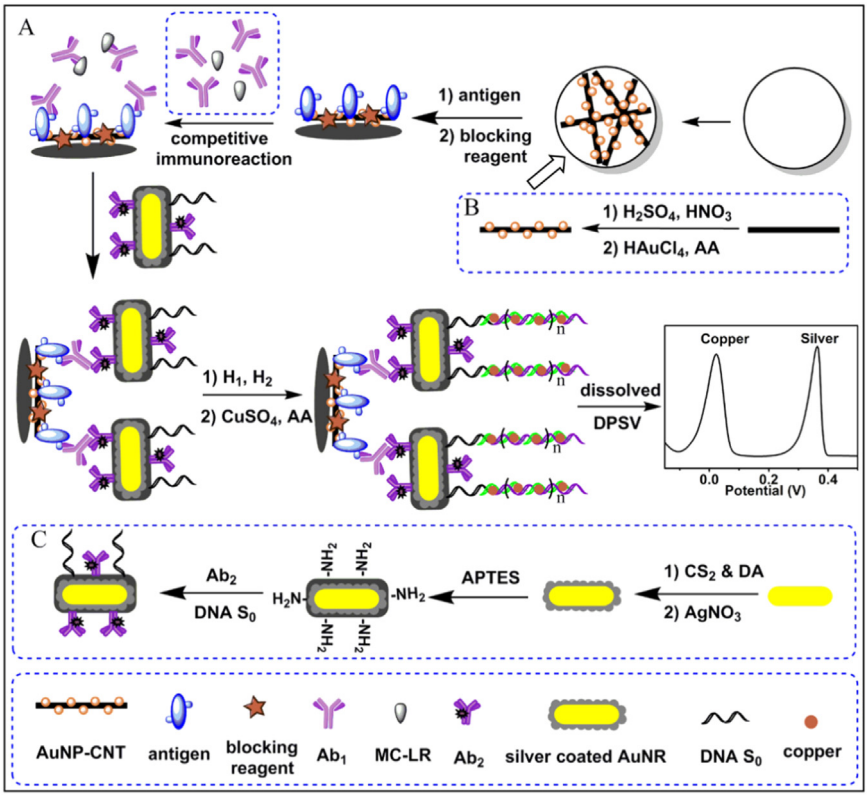

Scheme 1. Schematic immunoassay for the detection of MC-LR (A), the formation of AuNP-CNT composite (B) and the construction of S_0-AgNP/AuNR-Ab_2 (C).

2.4. Construction of the immunosensor

The illustration of the immunosensor was shown in Scheme 1A. Briefly, 60 μL of AuNP-CNT suspension containing 0.5% chitosan was dropped into 96-well microplate. After drying, 30 μL of diluted MC-LR antigen was added and incubated at 37 °C for 1 h, followed by 30 μL of 5% skim milk to block the nonspecific sites. An hour later, 30 μL mixture of Ab_1 and MC-LR was added, while the competitive immunoreaction with Ab_1 between the immobilized antigen and free MC-LR occurred. Subsequently, 30 μL of S_0-AgNP/AuNR-Ab_2 was added and incubated at 37 °C for another 1 h. To carry out HCR, hairpin oligonucleotides (H_1 and H_2) were firstly heated to 90 °C for 5 min and cooled down to room temperature. Then, 60 μL of hybridization buffer (50 mM PBS + 0.5 M NaCl, pH = 6.8) containing H_1 (2 μM) and H_2 (2 μM) was added and incubated for 1.5 h to form long dsDNA. After washing, 60 μL buffer solution (10 mM MOPS, 50 mM NaCl, 1 mM $MgCl_2$, pH = 7.5) containing 10 mM ascorbic acid and 0.5 mM $CuSO_4$ was added and incubated for 30 min, thus Cu NPs can be formed in dsDNA. Subsequently, 200 μL of 5 M nitric acid was added into the microplate for 10 min, thus Cu and Ag can be dissolved as Cu^{2+} and Ag^{+}, followed by transferring to 5 mL of 0.5 M HNO_3 solution. Finally, the DPSV was tested at the following conditions: potential range, −0.2–0.5 V; amplitude, 50 mV; pulse width, 0.05 s; pulse period, 0.5 s; deposition potential, −0.5 V; deposition time, 6 min.

3. Results and discussion

3.1. Characterization of AuNP-CNT composite

Due to the lack of functional groups and hydrophobic properties, raw CNTs were pretreated with concentrated sulfuric acid and nitric acid to produce carboxyl groups (Wang et al., 2017). In Fig. 1A, the ox-CNT showed integrated morphology without defects after acid-treatment, while in Fig. 1D, compared with the FT-IR of raw CNT, a broaden peak at about 3200 cm^{-1} by O-H stretching vibration and an obvious peak at 1718 cm^{-1} by C=O stretching vibration were found on the ox-CNT, indicating a higher amount of carboxyl groups of ox-CNT (Liu et al., 2011). Surprisingly, the water solubility of ox-CNT was tremendously improved since it can disperse in water homogeneously and steadily for at least two weeks, as shown in Fig. S1.

Traditional methods for AuNP-CNT composite include direct electrodeposition of Au on CNT (Wang et al., 2017) or the adsorption of AuNPs onto the surface of CNTs via electrostatic forces (Jiang et al., 2003). In view of the mild reducing property of ascorbic acid, an environmentally friendly one-step method was proposed to fabricate AuNP-CNT. From the TEM image of AuNP-CNT (Fig. 1B), AuNPs were uniformly anchored on the surface of CNTs without distinct aggregation, while the diameters of AuNPs were mostly between 20 and 30 nm (inset of Fig. 1B). Chitosan was frequently utilized in biosensors due to its outstanding performance including film-forming ability, good adhesion, high permeability and cheapness (Zhang et al., 2004b). Therefore, a small amount of chitosan was mixed up with AuNP-CNT to modify the substrate of the microplate. As the SEM in Fig. 1C, AuNP-CNT can be clearly found, implying that chitosan just served as adhesive without changing the property or structure of AuNP-CNT. The faveolate-like morphology of the nanocomposite, the high conductivity of CNTs and the strong protein-affinity of AuNPs provide abundant active sites for antigens.

To study the chemical composition of AuNP-CNT and the chemical status of Au element, the composite was measured by XPS. In the deconvolution of C 1 s (Fig. 1E), the characteristic peak at 284.5 eV was attributable to C=C/C-C for the carbon skeleton of ox-CNT (Su et al., 2017). In addition, the characteristic peaks observed at 286.3 eV and 288.5 eV were assigned to C-OH and O=C-O (Gobbo et al., 2013), respectively, which indicated that hydroxyl and carboxyl groups were generated on the surface of CNT. As for the deconvolution of O1s (Fig. 1F), the peaks at 531.8 eV and 533.1 eV were representative of the typical C=O and C-O groups (Gobbo et al., 2013). Therefore, the C1s and

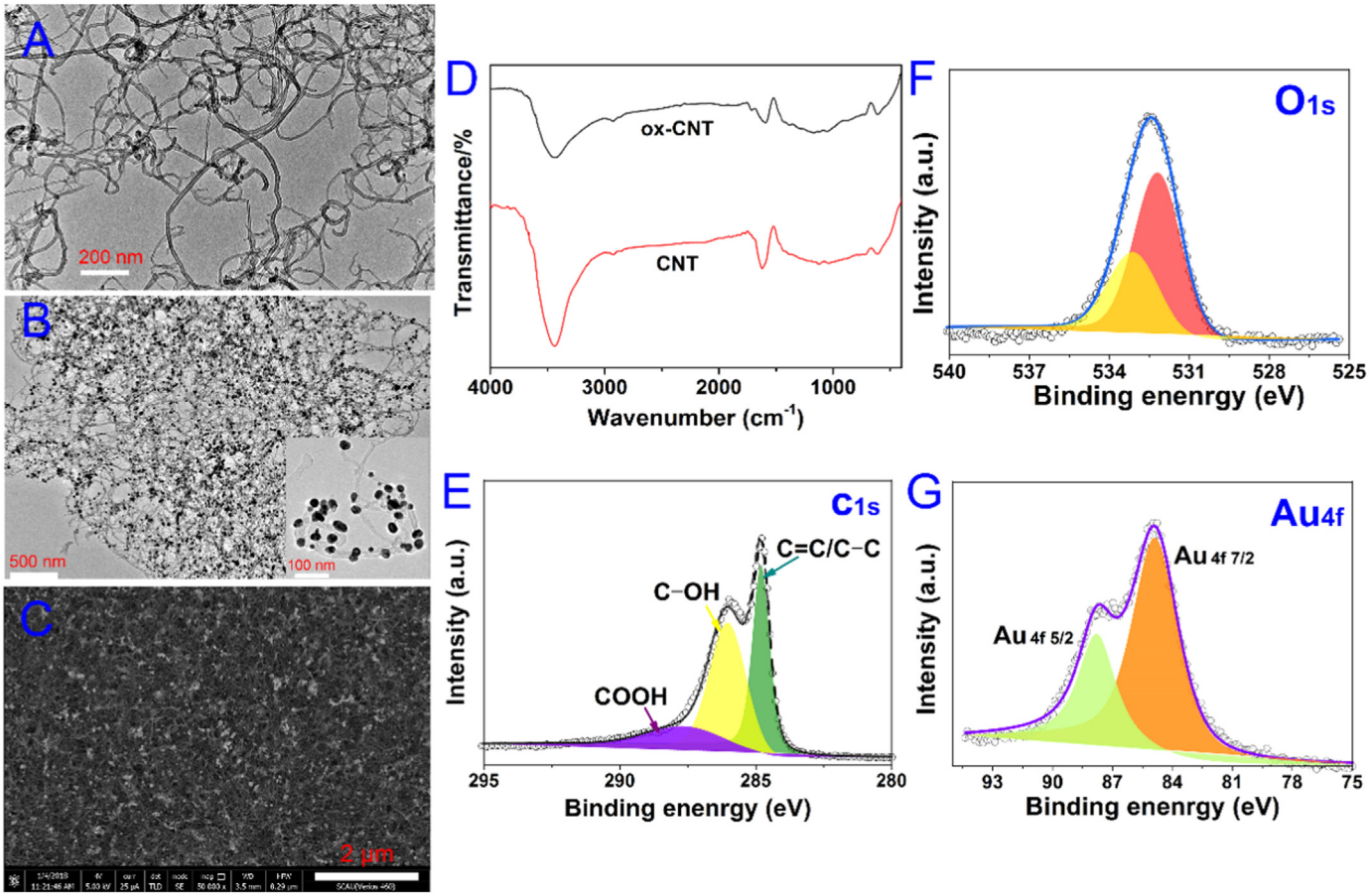

Fig. 1. TEM images of ox-CNT (A) and AuNP-CNT (B), SEM image of AuNP-CNT/chitosan (C), FT-IR spectra of CNT and ox-CNT (D), the deconvolution XPS of C1s (E), O1s (F) and Au4f (G).

O1s in XPS further verified the successful oxidation of CNTs, which was accordant with the FT-IR measurement. Furthermore, the deconvolution of Au 4f (Fig. 1G) showed two characteristic peaks at binding energies 84.5 eV and 87.5 eV corresponding to $Au_{4f7/2}$ and $Au_{4f5/2}$ components (Kwak et al., 2010), respectively, which suggests the presence of atomic gold. Therefore, the AuNP-CNT composite has been successfully synthesized.

3.2. Characterization of S_0-AgNP/AuNR-Ab_2 composite

In Fig. 2A, by a traditional seed-mediated method, the monodispersed AuNR showed a length of about 85 nm and a width of about 35 nm. DDTC (Fig. S2) with abundant sulfur atoms can covalently conjugate with AuNR by means of Au-S bond (Häkkinen, 2012). In Fig. 2B, about a thickness of 5 nm DDTC layer was found on the surface of AuNR, indicating the successful absorption of DDTC. Why should we introduce DDTC? Firstly, catechol groups on DDTC can be served as the chelating reagent to immobilize Ag^+ and also as reductive reagent to reduce Ag^+, thus Ag atoms can be formed on the AuNR. The discontinuous and inhomogeneous deposition for Ag atoms resulted in corn-like superstructures with AuNR core and AgNP shell. In order to obtain ideal AgNP/AuNR superstructure, the thickness of silver shell was adjusted by altering the amount of $AgNO_3$. When the volume of $AgNO_3$ was changed from 20 μL to 100 μL, the thickness of silver shell gradually increased, as shown in Fig. S3. However, it seemed that the silver shell thickness of 100 μL $AgNO_3$ did not increase remarkably when compared with that of 80 μL $AgNO_3$. From the optical photos in Fig. S3F, the product color changed from light green to deep orange when the volume of $AgNO_3$ was from 20 to 100 μL, whereas the color from 80 μL and 100 μL $AgNO_3$ was almost the same, indicating that 80 μL of $AgNO_3$ was enough. The elemental analysis in Fig. 2E and F showed obvious color contrast of Au (red) and Ag (green), proving that gold core was coated by silver shell perfectly, which was accorded with STEM image in Fig. 2D. In addition, the silver shell was about 21 nm thick (Fig. 2C), which can bring satisfactory electrochemical signal response. The UV–vis spectra in Fig. S4 showed that the longitudinal plasmon resonance wavelength of AgNP/AuNR (curve b) was red-shifted distinctly comparing with that of AuNR (curve a), confirming the successful synthesis of AgNP/AuNR.

Secondly, catechol groups on DDTC can react with APTES by silanization reaction (Crucho et al., 2016) to form amino groups on the surface of AgNP/AuNR. As shown in Fig. 2G, the amino-modified AgNP/AuNR still possessed certain dispersibility. Especially, the layer was about 3 nm (the inset in Fig. 2G). Such amino groups can be used to conjugate with secondary antibody and initiator DNA strand through Schiff base reaction. UV–vis spectra were performed to characterize the S_0-AgNP/AuNR-Ab_2 composite. As shown in Fig. 2H, the characteristic peaks located at 280 nm (curve a) and 260 nm (curve b) were attributed to Ab_2 and S_0, respectively. After covalently coupling with Ab_2 and S_0, the UV–vis absorption curve (curve d) of S_0-AgNP/AuNR-Ab_2 owned a broad peak near 270 nm due to Ab_2 and S_0, while a little movement at 520 nm and 710 nm suggested that the association of Ab_2 and S_0 influence the adsorption of amino-modified AgNP/AuNR (curve c). Besides, the surface chemistry property was further analyzed. As shown in Fig. 2I, the zeta potential of amino-modified AgNP/AuNR was about 26.1 mV in pH = 7.0 buffer solution due to the positive electrical property of amino groups. However, after association with biomolecules, it was changed negatively about −29.3 mV due to the negative carboxyl groups of Ab_2 and the phosphate backbone of DNA. Therefore, both the UV–vis absorption and zeta potential characterization provide

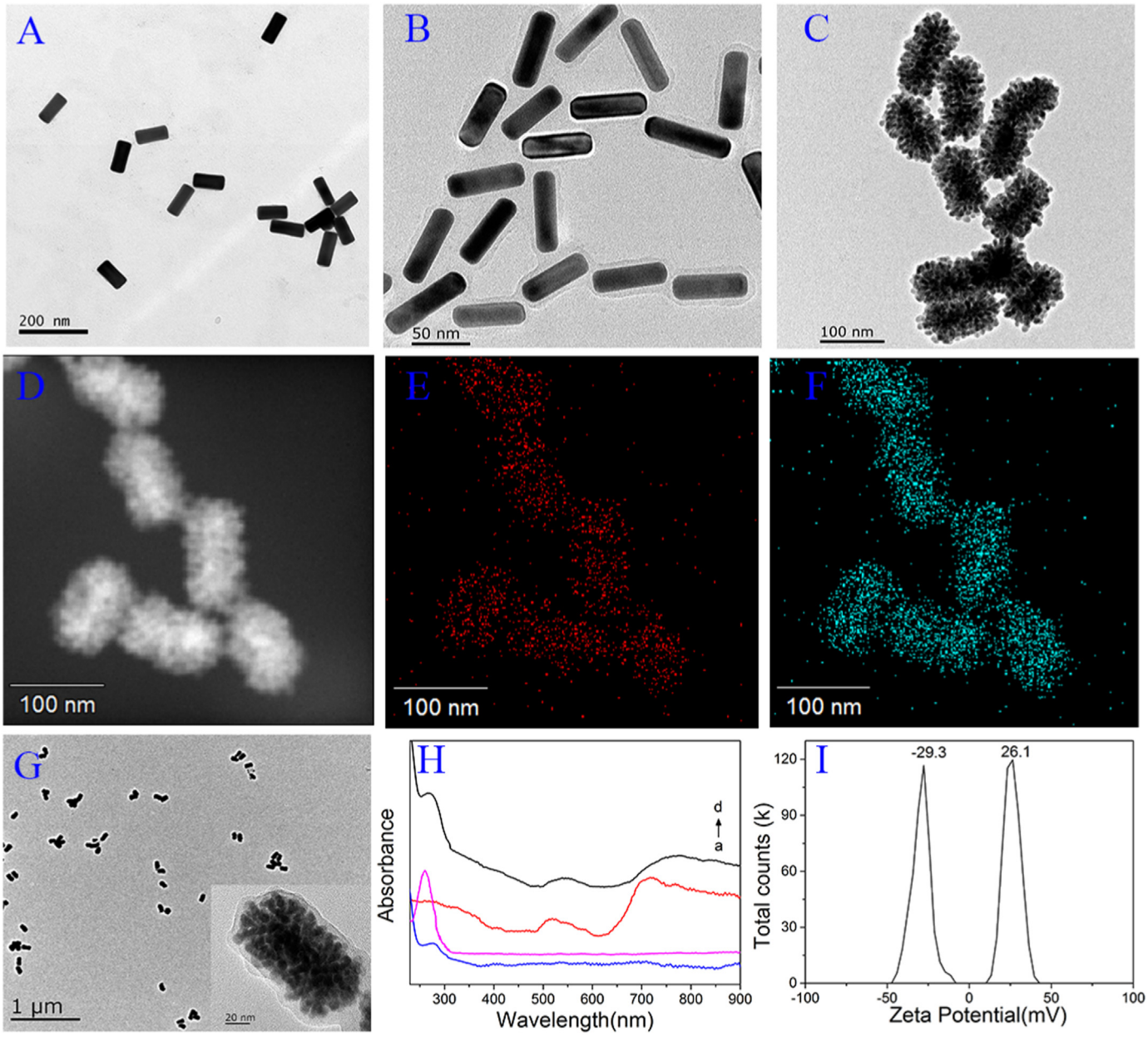

Fig. 2. TEM images of AuNR (A), DDTC-AuNR (B), AgNP/AuNR (C); STEM image of AgNP/AuNR (D), elemental mapping of gold (E) and silver (F); TEM image of amino-modified AgNP/AuNR (G). (H) UV–vis spectra of Ab_2 (a), initiator DNA strand (b), amino-modified AgNP/AuNR (c) and S_0-AgNP/AuNR-Ab_2 (d). (I) Zeta potential of amino-modified AgNP/AuNR (right) and S_0-AgNP/AuNR-Ab_2 (left).

synergistic evidence for the assembly of S_0-AgNP/AuNR-Ab_2.

3.3. Assembly and feasibility of the immunoassay

This immunoassay process was shown in Scheme 1A. Electrochemical impedance spectroscopy (EIS) was performed to monitor the whole fabricated process. It was carried out in 5 mM $[Fe(CN)_6]^{3-/4-}$ solution containing 0.1 M KCl, with a bias potential of 0.2 V, a frequency range of 0.1–100 kHz and an amplitude of 50 mV. The Nyquist diagrams of different immunosensors were shown in Fig. 3A, where the inset was the equivalent circuit model. The semicircle diameter corresponding to the high frequency represents the electrode surface charge transfer resistance (R_{ct}). When the electron transfer was limited, a larger semicircle diameter was achieved (Chen et al., 2010). Compared with bare ITO (curve a), the semicircle diameter (curve b) decreased obviously due to the excellent conductivity of AuNP and CNT when the AuNP-CNT composite was modified. After the antigen was immobilized, the electrode surface charge transfer (curve c) was limited, resulting in a bigger semicircle diameter, indicating the successful absorption of antigen. The diameters of the high frequency further increased (curve d-f) when blocking reagent, Ab_1 and S_0-AgNP/AuNR-Ab_2 were immobilized, since these biomaterials obstructed the electron transfer, suggesting that the immunoreaction was accomplished. After hybridization chain reaction, long DNA double strands were generated to prevent the transfer of $[Fe(CN)_6]^{3-/4-}$ redox probe due to their negative charges, thus the semicircle diameter increased notably.

The immunoassay was implemented in 96-well microplate, since it is easy to dissolve metals by treating with 5 M nitric acid, and then the electrochemical signal was recorded through DPSV. The electrodeposition is very important in the detection of metal ions. As in Fig. 3B, the DPSV before (curve a) and after (curve b) electrodeposition were compared, suggesting that the peak currents of both copper (about

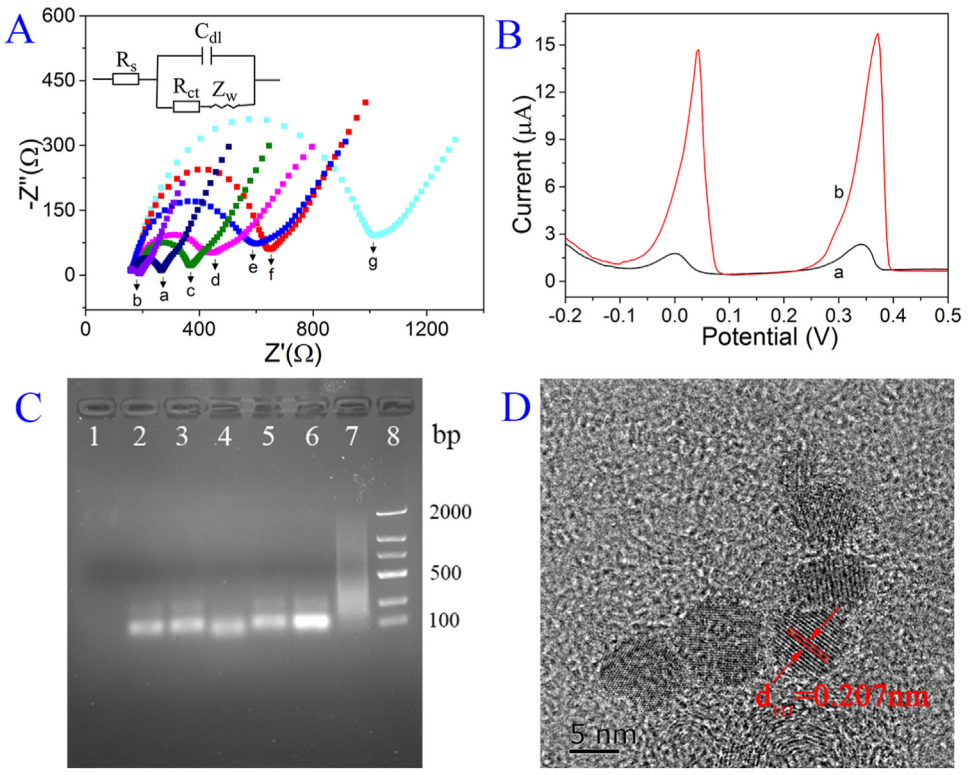

Fig. 3. (A) EIS for different electrodes, bare ITO (a) and further modified with AuNP-CNT (b), antigen (c), blocking reagent (d), Ab_1 (e), S_0-AgNP/AuNR-Ab_2 (f), HCR (g); (B) DPSV before (curve a) and after (curve b) electrodeposition for a complete immunoassay process; (C) Agarose gel electrophoresis images: S_0 (1), H_1 (2), H_2 (3), S_0 + H_1 (4), S_0 + H_2 (5), H_1 + H_2 (6), S_0 + H_1 + H_2 (7) and DNA marker (8); (D) HRTEM image of HCR product induced-formation of Cu NPs.

0.03 V) and silver (about 0.35 V) were obviously enhanced. Therefore, an electrodeposition procedure was performed before DPSV of metal ions, since pre-concentration is an effective way to improve the signal response and further enhance determination sensitivity (Zhu et al., 2016).

In addition, HCR product was confirmed by agarose gel electrophoresis, where 1.5% agarose gel was prepared in 0.5 × TBE buffer, 4S Green nucleic acid was used as stain and the gel was run at a potential of 120 V for 1 h. As shown in Fig. 3C, lane 1–8 represented S_0, H_1, H_2, mixture of S_0 + H_1, S + H_2, H_1 + H_2, S_0 + H_1 + H_2 and DNA marker, respectively. S_0 was so short that it escaped from the agarose gel (lane 1). On the contrary, H_1 or H_2 was stable when existed alone (lane 2 and 3). Besides, when initiator DNA strand was mixed with H_1 or H_2 (lane 4 and 5), there was no obvious strip compared with the single lane of H_1 and H_2. Compared lane 6 with lane 7, it meant that the hybridization chain reaction can only occur when S_0, H_1 and H_2 co-existed. The HCR product was generated as the template for the formation of Cu NPs. As shown in TEM image (Fig. 3D), the diameters of Cu NPs were about 7 nm, where the interplanar crystal spacing of 0.207 nm was due to the (111) plane of metallic copper (Tang et al., 2015).

3.4. Optimization of the experimental conditions

Several experiment conditions that could significantly affect the performance of the immunoassay such as the concentration of antigen and Ab_1, time for HCR, concentration of cupric ion and deposition time for DPSV were investigated in detail. As for an electrochemical immunoassay, the immobilized amount of antigen or antibody upon substrate platform played an important part in the immunosensor. When the active sites of immobilized surface were not occupied completely, large background signal to noise may appear. Here, only S_0-AgNP/AuNR-Ab_2 was used in this step and the signal response was recorded from the DPSV peak current of silver. As shown in Fig. 4A, the peak current increased when the dilution ratio of antigen increased from 1:1200 to 1:100. The dilution ratio of 1:50 may be excessive since it may result in the instability for the immunoassay, so 1:100 was an optimal dilution ratio for antigen. The concentration of Ab_1 can also influence the performance of the immunoassay. Based on the competitive detection of MC-LR, low concentration of Ab_1 may narrow the detection linear range, while saturate concentration may decline the sensitivity of competitive immunoassay. As shown in Fig. 4B, when the dilution ratio of Ab_1 increased from 1:1600 to 1:100, the peak current raised gradually. It seemed that the dilution ratio of 1:100 was a saturate concentration, thus 1:200 was selected.

In this immunoassay, the DPSV peak current from Cu^{2+} was another signal response. Cu NPs were generated in DNA double helix of HCR product. Longer the DNA was, more sites for Cu NPs. When HCR time increased from 15 to 90 min, the peak current of copper increased gradually, shown in Fig. 4C. But the peak current of copper no longer increased when HCR time was more than 90 min, suggesting that the substrate of HCR was entirely consumed. Therefore, 90 min was enough for HCR. In addition, Cu NPs were reduced from copper sulfate, so the concentration of cupric ion affected the formation of copper particles. As shown in Fig. 4D, the peak current gradually increased when the concentration of Cu^{2+} changed from 0.1 to 0.5 mM, and reached a plateau after 0.5 mM. Consequently, the optimum concentration of cupric ion was selected as 0.5 mM.

The pre-concentration process can accumulate the amount of silver and copper onto the electrode surface. In this step, the dual-signal readout was recorded from DPSV measurement of silver and copper. The deposition time was studied, as shown in Fig. 4E. The peak currents of both silver (top) and copper (down) increased as the deposition time. The peak current of silver reached a plateau at a deposition time of 4 min, while that of copper achieved a plateau at a deposition time of 6 min. So, the deposition time of 6 min was chosen as the optimal accumulation time.

3.5. The performance of the immunosensor

The AuNP-CNT composite was utilized as the substrate material to immobilize MC-LR antigen and S_0-AgNP/AuNR-Ab_2 was used as nanocarrier to trigger hybridization chain reaction. In the meanwhile, a

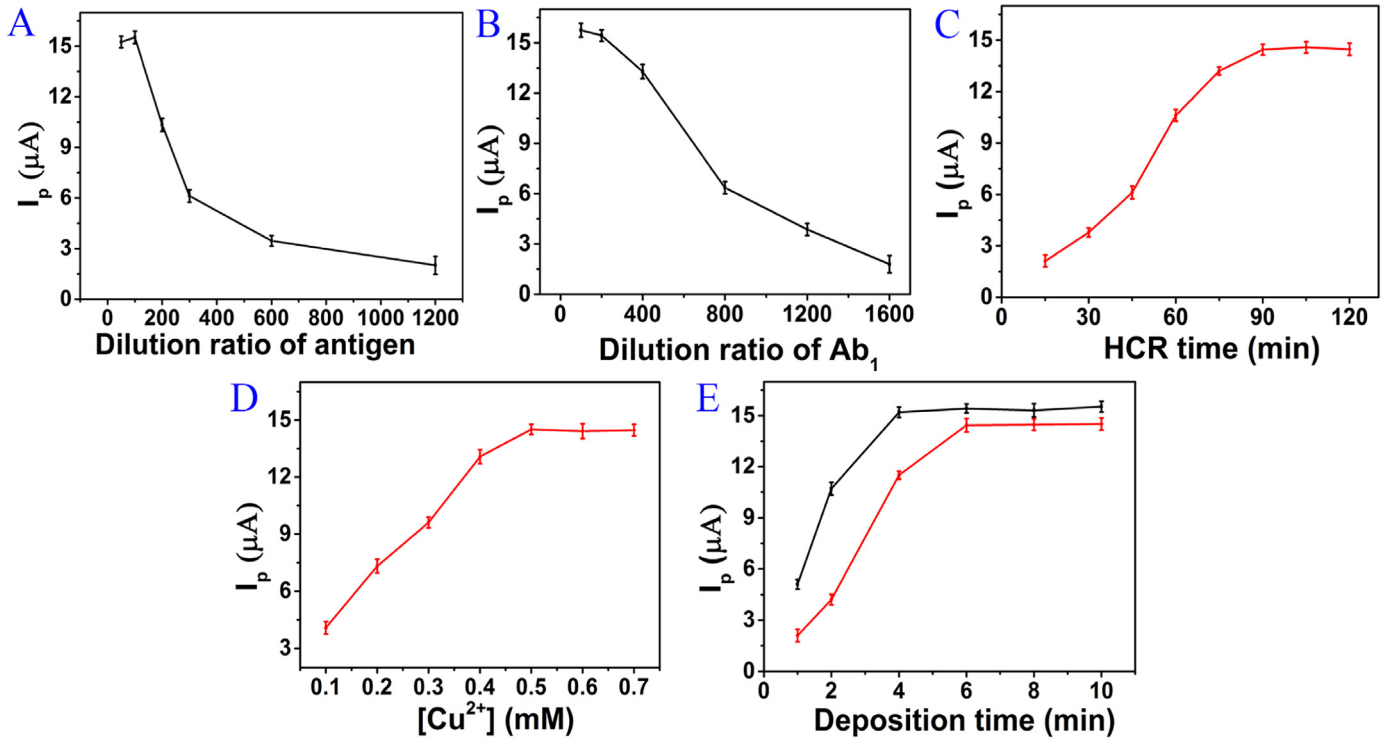

Fig. 4. Effect of the dilution ratio of antigen (A) and primary antibody (B), reaction time for HCR (C), concentration of Cu^{2+} (D), and deposition time for DPSV measurement of silver (top) and copper (bottom) (E).

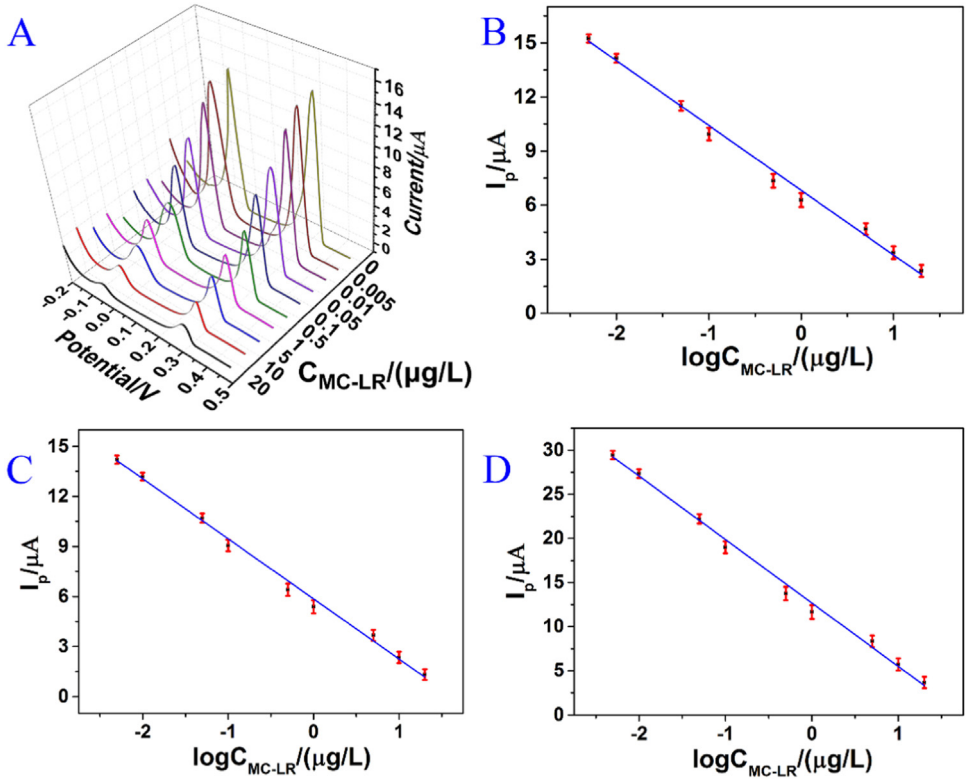

Fig. 5. (A) Dynamic DPSV curves of the immunoassay for different concentrations of MC-LR, and the linear response of the electrochemical peak currents of silver (B), copper (C) and both silver and copper (D) with the concentration.

competitive immunoassay was performed to detect MC-LR. A series of MC-LR solutions with known concentrations were mixed with a certain amount of Ab_1 and then dropped into the microplate, thus the immobilized antigen on the microplate and MC-LR in the mixture can compete to react with Ab_1. When the concentration of MC-LR increased, the DPSV signals of both silver and copper decreased since less amount of Ab_1 was immobilized with the antigen. Under the optimum conditions, the dynamic electrochemical responses between peak currents

and concentrations were shown in Fig. 5A. The calibration curves between Ip of silver/copper and the logarithmic concentration of MC-LR were shown in Fig. 5B and C. In a range from 0.005 to 20 μg/L, as for the individual silver DPSV signal (Fig. 5B), the linear regression equation was Ip(Ag) = 6.85–3.57 × $\log C_{MC\text{-}LR}$, (R^2 = 0.996), of which the detection limit was 3.2 ng/L, while as for individual copper DPSV signal (Fig. 5C), the linear regression equation was Ip(Cu) = 5.96–3.53 × $\log C_{MC\text{-}LR}$ (R^2 = 0.995), of which the detection limit was 3.3 ng/L. Furthermore, the peak currents of silver and copper were summed, which also showed a relationship with the logarithmic concentration of MC-LR in Fig. 5D. The linear regression equation was Ip(Ag + Cu) = 12.52–7.04 × $\log C_{MC\text{-}LR}$ (R^2 = 0.996), of which the detection limit was 2.8 ng/L. It was observed that the LOD of dual-signal readout was little lower than each single-signal readout method, since the combination of the currents was an effective way to amplify the signal response to improve the detection sensitivity (Wu et al., 2013). As in Table S1, the wide linear range and low detection limit of this immunoassay was better than or comparable with reported works. The possible reasons for the excellent performance of such immunoassay were as follows. (1) DPSV is an effective electrochemical technique that can increase detection sensitivity (Guha et al., 2014); (2) The cascade hybridization chain reaction strategy was available in improving determination sensitivity and decreasing the limit of detection; (3) Multi-signal readout was a promising way to lower the limit of detection (Yu et al., 2016).

3.6. Reproducibility, specificity and stability of the immunoassay

The reproducibility of the proposed immunoassay was investigated. Five parallel experiments were performed to detect 0.1, 1 and 5 μg/L of MC-LR. By recording and comparing the DPSV peak current of silver, the intra-assay coefficient variations were 3.8%, 3.2% and 3.4% respectively, indicating a good precision and reproducibility.

The specificity of the immunoassay was evaluated by detecting MC-LR while its analogues coexisted. When experiments were performed to analyze 1 μg/L of MC-LR, equal concentration of MC-RR, MC-YR and nodularin was added, respectively. The DPSV current from silver remained 95.3–98.1% when only one interferent existed. It was still maintained 92.6% while three interferents existed, as shown in Fig. S5, indicating acceptable specificity of the immunoassay.

In addition, the stability of the immunoassay was evaluated by the DPSV peak current of silver. When the AuNP-CNT modified microplate was stored at 4 °C for two weeks, the DPSV peak current remained 93.2%. When the S_0-AgNP/AuNR-Ab_2 conjugation was stored at 4 °C for two weeks, the peak current only decreased 4.5% comparing with the fresh preparation. So the stability of the developed immunoassay was also accepted.

3.7. Recovery test

The practical application test was performed through standard addition method by using Poyang lake water in South China Agricultural University and tap water as real water sample. The spiked concentrations of MC-LR were 0.1, 1 and 10 μg/L, and the recoveries were in the range from 94.2% to 107.0%, as shown in Table S2. The acceptable results indicated that the developed method was feasible to monitor MC-LR in real water samples.

4. Conclusion

In this work, a dual-signal readout electrochemical immunoassay was fabricated to detect MC-LR. A one-step method was introduced to synthesize AuNP-CNT composite that was used as substrate platform to immobilize MC-LR antigen. Furthermore, the corn-like AgNP/AuNR superstructure was functionalized as nanocarrier to capture secondary antibody for the immunoreaction and initiator DNA strand for the hybridization chain reaction, while the long DNA chains provided sites to generate copper nanoparticles. By converging HCR technique and AgNP/AuNR carrier, the dual-signal readout immunoassay from the DPSV of silver and copper was used to reflect the concentrations of MC-LR, where such dual-signal readout can support each other to provide a more convincible signal, but also improve the detection limit. The proposed method exhibited good reproducibility, specificity and stability, and its recoveries from real water sample were acceptable as well. This enzyme-free dual-signal method may provide new tactics to build novel and stable immunosensor for further use, such as environmental monitoring and clinical diagnosis.

Acknowledgments

This work was supported by the National Natural Science Foundation of China (21475047, 21705051, 21874048), the Science and Technology Planning Project of Guangdong Province (2016B030303010), the Scientific Foundation of Guangdong Province (2017A030313077), National Key Research and Development Program of China (SQ2017YFC160089), the Program for the Top Young Innovative Talents of Guangdong Province (2016TQ03N305), the Science and Technology Innovation Project of Guangdong University Students (pdjhb0086), the Foundation for High-level Talents in South China Agricultural University and Central Public-interest Scientific Institution Basal Research Fund for Chinese Academy of Tropical Agricultural Sciences (1630122017011, 1630122017009).

Appendix A. Supporting information

Supplementary data associated with this article can be found in the online version at doi:10.1016/j.bios.2018.10.033.

References

Alagiri, M., Rameshkumar, P., Pandikumar, A., 2017. Microchim. Acta 184 (9), 3069–3092.
Chen, J., Zhang, J., Yang, H., Fu, F., Chen, G., 2010. Biosens. Bioelectron. 26 (1), 144–148.
Chikkaveeraiah, B.V., Bhirde, A.A., Morgan, N.Y., Eden, H.S., Chen, X., 2012. ACS Nano 6 (8), 6546–6561.
Crucho, C.I.C., Baleizão, C., Farinha, J.P.S., 2016. Anal. Chem. 89 (1), 681–687.
Dai, L., Song, L., Huang, Y., Zhang, L., Lu, X., Zhang, J., Chen, T., 2017. Langmuir 33 (22), 5378–5384.
Dirks, R.M., Pierce, N.A., 2004. Proc. Natl. Acad. Sci. USA 101 (43), 15275–15278.
Du, D., Zou, Z., Shin, Y., Wang, J., Wu, H., Engelhard, M.H., Liu, J., Aksay, I.A., Lin, Y., 2010. Anal. Chem. 82 (7), 2989–2995.
Felix, F.S., Angnes, L., 2018. Biosens. Bioelectron. 102, 470–478.
Gan, C., Ling, L., He, Z., Lei, H., Liu, Y., 2016. Biosens. Bioelectron. 78, 381–389.
Ge, Y., Wu, J., Ju, H., Wu, S., 2014a. Talanta 120, 218–223.
Ge, Z., Lin, M., Wang, P., Pei, H., Yan, J., Shi, J., Huang, Q., He, D., Fan, C., Zuo, X., 2014b. Anal. Chem. 86 (4), 2124–2130.
Gobbo, P., Biesinger, M.C., Workentin, M.S., 2013. Chem. Commun. 49 (27), 2831–2833.
Guha, K.S., Mascarenhas, R.J., Thomas, T., D Souza, O.J., 2014. Ionics 20 (6), 849–856.
Häkkinen, H., 2012. Nat. Chem. 4 (6), 443–455.
Halvorson, R.A., Vikesland, P.J., 2011. Environ. Sci. Technol. 45 (13), 5644–5651.
Jeong, B., Akter, R., Han, O.H., Rhee, C.K., Rahman, M.A., 2013. Anal. Chem. 85 (3), 1784–1791.
Jiang, K., Eitan, A., Schadler, L.S., Ajayan, P.M., Siegel, R.W., 2003. Nano Lett. 3 (3), 275–277.
Jung, J.H., Cheon, D.S., Liu, F., Lee, K.B., Seo, T.S., 2010. Angew. Chem. Int. Ed. 49 (33), 5708–5711.
Karci, A., Wurtzler, E.M., de la Cruz, A.A., Wendell, D., Dionysiou, D.D., 2018. J. Hazard. Mater. 349, 282–292.
Kokkinos, C., Economou, A., Prodromidis, M.I., 2016. Trend Anal. Chem. 79, 88–105.
Kwak, I.S., Bae, M.A., Won, S.W., Mao, J., Sneha, K., Park, J., Sathishkumar, M., Yun, Y., 2010. Chem. Eng. J. 165 (2), 440–446.
Lai, G., Wang, L., Wu, J., Ju, H., Yan, F., 2012. Anal. Chim. Acta 721, 1–6.
Lai, G., Wu, J., Ju, H., Yan, F., 2011. Adv. Funct. Mater. 21 (15), 2938–2943.
Lin, D., Wu, J., Wang, M., Yan, F., Ju, H., 2012. Anal. Chem. 84 (8), 3662–3668.
Lin, Y., Zhou, Q., Lin, Y., Lu, M., Tang, D., 2015. Anal. Chim. Acta 887, 67–74.
Liu, X., Sun, X., Huang, Y., Sheng, G., Wang, S., Yu, H., 2011. Energy Environ. Sci. 4 (4), 1422.
Mehta, V.N., Kumar, M.A., Kailasa, S.K., 2013. Ind. Eng. Chem. Res. 52 (12), 4414–4420.
Noble, J.E., Ganju, P., Cass, A.E.G., 2003. Anal. Chem. 75 (9), 2042–2047.
Peng, J., Feng, L., Ren, Z., Jiang, L., Zhu, J., 2011. Small 7 (20), 2921–2928.

Pham, T., Utsumi, M., 2018. J. Environ. Manag. 213, 520–529.
Pivetal, J., Pereira, F.M., Barbosa, A.I., Castanheira, A.P., Reis, N.M., Edwards, A.D., 2017. Analyst 142 (6), 959–968.
Qileng, A., Yang, S.Y., Wei, J., Lu, N., Lei, H.T., Liu, Y.J., Liu, W.P., 2018a. Sens. Acutators B-Chem. 267, 216–223.
Qileng, A., Wei, J., Lu, N., Cai, Y., Chen, M.S., Lei, H.T., Liu, Y.J., 2018b. Biosens. Bioelectron. 106, 219–226.
Ríos, V., Moreno, I., Prieto, A.I., Puerto, M., Gutiérrez-Praena, D., Soria-Díaz, M.E., Cameán, A.M., 2013. Food Chem. Toxicol. 57, 170–178.
Rotaru, A., Dutta, S., Jentzsch, E., Gothelf, K., Mokhir, A., 2010. Angew. Chem. Int. Ed. 49 (33), 5665–5667.
Shen, W., Zhuo, Y., Chai, Y., Yang, Z., Han, J., Yuan, R., 2015. ACS Appl. Mater. Inter. 7 (7), 4127–4134.
Song, C., Yang, X., Wang, K., Wang, Q., Huang, J., Liu, J., Liu, W., Liu, P., 2014. Anal. Chim. Acta 827, 74–79.
Su, D., Cortie, M., Wang, G., 2017. Adv. Energy Mater. 7 (8), 1602014.
Sun, Z., Luo, Z., Gan, C., Fei, S., Liu, Y., Lei, H., 2014. Biosens. Bioelectron. 59, 99–105.
Tang, Q., Yang, T., Huang, Y., 2015. Microchim. Acta 182 (13–14), 2337–2343.
Wan, Y., Lin, Z., Zhang, D., Wang, Y., Hou, B., 2011. Biosens. Bioelectron. 26 (5), 1959–1964.
Wang, H., Yao, S., Liu, Y., Wei, S., Su, J., Hu, G., 2017. Biosens. Bioelectron. 87, 417–421.
Wu, L., Zhang, X., Liu, W., Xiong, E., Chen, J., 2013. Anal. Chem. 85 (17), 8397–8402.
Xu, F., Shi, H., He, X., Wang, K., He, D., Guo, Q., Qing, Z., Yan, L.A., Ye, X., Li, D., Tang, J., 2014. Anal. Chem. 86 (14), 6976–6982.
Yang, Z., Jiang, W., Liu, F., Zhou, Y., Yin, H., Ai, S., 2015. Chem. Commun. 51 (78), 14671–14673.
Yin, H., Wang, H., Jiang, W., Zhou, Y., Ai, S., 2017. Biosens. Bioelectron. 90, 494–500.
Yu, P., Liu, Y., Zhang, X., Zhou, J., Xiong, E., Li, X., Chen, J., 2016. Biosens. Bioelectron. 79, 22–28.
Zhang, L., Ping, X., Yang, Z., 2004a. Talanta 62 (1), 191–198.
Zhang, M., Smith, A., Gorski, W., 2004b. Anal. Chem. 76 (17), 5045–5050.
Zhao, Y., Zheng, Y., Kong, R., Xia, L., Qu, F., 2016. Biosens. Bioelectron. 75, 383–388.
Zhu, Y., Wang, H., Wang, L., Zhu, J., Jiang, W., 2016. ACS Appl. Mater. Interface 8 (4), 2573–2581.